



Materials for flexible bioelectronic systems as chronic neural interfaces

Enming Song^{1,14}, Jinghua Li^{2,3,14}, Sang Min Won^{4,14}, Wubin Bai^{5,14} and John A. Rogers^{1,5,6,7,8,9,10,11,12,13} ✉

Engineered systems that can serve as chronically stable, high-performance electronic recording and stimulation interfaces to the brain and other parts of the nervous system, with cellular-level resolution across macroscopic areas, are of broad interest to the neuroscience and biomedical communities. Challenges remain in the development of biocompatible materials and the design of flexible implants for these purposes, where ultimate goals are for performance attributes approaching those of conventional wafer-based technologies and for operational timescales reaching the human lifespan. This Review summarizes recent advances in this field, with emphasis on active and passive constituent materials, design architectures and integration methods that support necessary levels of biocompatibility, electronic functionality, long-term stable operation in biofluids and reliability for use in vivo. Bioelectronic systems that enable multiplexed electrophysiological mapping across large areas at high spatiotemporal resolution are surveyed, with a particular focus on those with proven chronic stability in live animal models and scalability to thousands of channels over human-brain-scale dimensions. Research in materials science will continue to underpin progress in this field of study.

Implantable bioelectronic systems that provide long-term, active functionality at soft biotissue interfaces represent powerful tools for biomedical research; they also have the potential to form the foundations for engineering approaches to the treatment of disease^{1,2}. Of particular interest are advanced platforms that offer sophisticated modes of operation enabled by distributed collections of semiconductor components as electrical/optical interfaces across a range of spatiotemporal scales^{3,4}. Here, progress in materials science establishes the basis for the seamless integration of microsystems technologies with living organisms, to provide persistent, multimodal function with applications in monitoring and modulating cardiac cycles, mapping and stimulating neural circuits, regenerating sensorimotor functions and many others^{5–8}. The most mature devices approved for widespread use in humans, such as deep-brain stimulators, cochlear implants, cardiac pacemakers and others, all employ similar engineering designs^{9,10}. In such systems, electronic modules sealed in stiff, rigid housings to isolate them from the surrounding biology connect through insulated wires to metal electrodes that serve as biotissue interfaces. Despite their essential value in treating patients worldwide, these basic architectures do not provide scalable routes to large numbers (hundreds or thousands, or more) of interface points nor do they allow for contact across large, curved surfaces or extended volumetric spaces. Alternative platforms with superior function and demonstrated utility as interfaces to the brain involve dense arrays of penetrating conductive needles on silicon wafer platforms (so-called Utah arrays)¹¹, distributed collections of passive electrodes on flexible sheets for electrocorticography (ECoG)¹² and linear sets of electrodes on narrow filaments (so-called Michigan probes)¹³. The first of these types of devices,

commonly exploited in brain/machine interfaces, incorporates individually addressable electrical probes of doped silicon (~0.5–1.5 mm long, ~40–100 μm wide)^{14–16}. The second, sometimes used as diagnostic tools in surgical procedures for epilepsy, often incorporates platinum electrodes (~2 mm diameter) in two-dimensional arrays on silicone substrates (area of 4 × 4 cm², 1 mm thick)¹². The third, frequently leveraged in neuroscience studies, relies on silicon shanks, typically 3 mm long, 50 μm wide and 15 μm thick with lithographically patterned electrodes distributed along their lengths¹⁷. These three platforms offer powerful capabilities, but their lack of active semiconductor functionality in proximity to the biotissue interface and, in some cases, their non-ideal mechanical properties, geometric layouts and/or integration approaches, limit the performance, scalability and ability to deploy into or onto biological systems of interest.

Recent and conceptually distinct types of bioelectronic/optoelectronic devices take the form of functional thin-film membranes, flexible filaments and open network meshes^{18–20}, with powerful possibilities in levels of functional integration. Here, large-scale arrays of active components, sometimes with thousands of independent channels, establish direct biotissue/electronic contacts^{21,22}. Some of the most notable recent advances involve demonstrations of safe, chronic operation in vivo^{3,23}, in freely moving and behaving animals. Key enabling features are biocompatible constituent materials, ‘perfect’ biofluid barrier coatings and mechanically compliant architectures, all in the context of hybrid, integrated platforms that induce minimal immune responses and biotissue damage but support device performance characteristics that match, in some cases, those of conventional planar electronic/optoelectronic systems

¹Center for Bio-Integrated Electronics, Northwestern University, Evanston, IL, USA. ²Department of Materials Science and Engineering, The Ohio State University, Columbus, OH, USA. ³Center for Chronic Brain Injury, The Ohio State University, Columbus, OH, USA. ⁴Department of Electrical and Computer Engineering, Sungkyunkwan University, Suwon, Republic of Korea. ⁵Department of Materials Science and Engineering, Northwestern University, Evanston, IL, USA. ⁶Department of Biomedical Engineering, Northwestern University, Evanston, IL, USA. ⁷Department of Neurological Surgery, Northwestern University, Evanston, IL, USA. ⁸Department of Chemistry, Northwestern University, Evanston, IL, USA. ⁹Department of Mechanical Engineering, Northwestern University, Evanston, IL, USA. ¹⁰Department of Electrical Engineering, Northwestern University, Evanston, IL, USA. ¹¹Department of Computer Science, Northwestern University, Evanston, IL, USA. ¹²Feinberg School of Medicine, Northwestern University, Evanston, IL, USA. ¹³Querrey-Simpson Institute for Bioelectronics, Northwestern University, Evanston, IL, USA. ¹⁴These authors contributed equally: Enming Song, Jinghua Li, Sang Min Won, Wubin Bai. ✉e-mail: jrogers@northwestern.edu

on rigid, planar semiconductor wafers^{24,25}. Examples of the most sophisticated platforms of this type use thin active materials/devices in shape-conformal layouts as the basis for amplified sensing and multiplexed addressing in spatiotemporally resolved electrophysiological interfaces to surfaces of the heart and brain, as well as into the depths of these organs^{18,21,22}. In all cases, a persistent challenge is in the prevention of biofluid penetration into the active electronic components to avoid associated degradation from corrosion of the functional materials and biological damage from leakage of electrical currents into surrounding biotissues. The ultimate demands are for coatings with zero permeability to water over timescales of many decades (lifetime of the patient), and with thicknesses in the sub-micrometre regime. Bulk containment housings like those used for conventional implants are clearly not applicable. The broad central focus in materials science that encompasses all of these considerations is in the development of complete collections of biocompatible materials with passive, active, barrier and interface functionality, along with associated schemes in materials processing and assembly.

Recently reported classes of flexible electronic materials, ranging from thin-film polymers for active electrophysiological recordings^{21,25} to multilayer stacks of inorganic/organic films for organic light-emitting diode displays^{26,27}, are of potential interest. Daunting challenges remain, however, in the use of such materials to achieve high-performance operation and chronic stability in bioelectronics. The combined effects of intrinsic and extrinsic limitations, ranging from comparatively poor charge transport characteristics, finite rates of water permeation and poor structural properties (such as pinholes, cracks and grain boundaries), represent some of the most notable aspects that require further improvements. As a result, flexible, active bioelectronic systems that offer chronic, high-performance operation and rely exclusively on polymers for the primary active components and biofluid barriers may prove to be difficult to realize.

This Review summarizes recent progress in schemes that combine organic with inorganic materials in hybrid platforms with the necessary operational features and in a broad range of unusual form factors. The emphasis is on engineered materials, device designs and integration methods with proven utility in live animal models, as high-performance and chronically stable interfaces to the brain, with additional potential for application to the peripheral nerves, the spinal cord, the heart and others. Subsequent sections review different classes of flexible materials for these purposes, followed by comparative evaluation of various processing strategies, with some focus on physically transferred ultrathin membranes that have submicrometre thicknesses. Additional discussions highlight examples of actively multiplexed, amplified bioelectronic systems that support record levels of spatiotemporal resolution in electrophysiological mapping and stimulation. The most recent devices incorporate tens of thousands of active unit cells distributed with variable densities across full organ-scale dimensions. The focus encompasses emerging technologies and material strategies for bioelectronic systems as chronic neural interfaces, many of which offer potential for immediate use in fundamental research studies, at the level of cell cultures, to organoids, and to animal models. As such, the content is not confined to approaches that currently have straight or clearly defined paths to specific uses in humans, sometimes an ultimate goal but often not the only aim of research in this area. Overall, this Review provides a framework for considering additional, materials-oriented advances in these systems. Successful research efforts in these areas could provide the basis for future generations of conformal, bioelectronic implants with long-lived high-performance operation.

Implantable platforms for stable biocompatibility

Bioelectronic implants with chronic stability are of growing importance in biomedical research and clinical medicine, with capabilities

that can include both sensing and stimulation. Development efforts typically focus on high-fidelity biotic/abiotic interfaces, achieved through a combination of advanced materials, mechanical constructs, shapes and layouts, and surface coatings that ensure biocompatibility, low-impedance interfaces and stable operation. An important feature is the design of unique form factors with geometries and mechanics that are compatible with those of targeted biotissues for minimally invasive implantation and subsequent chronic use. Overall device miniaturization can provide additional important benefits, in a manner that avoids substantial biotissue damage and scar formation and thus enhances operational stability. Figure 1 presents a collection of some recent examples, in layouts that range from flexible filamentary probes (Fig. 1a–c), to sheet-like architectures (Fig. 1d–f) and to open-mesh geometries (Fig. 1g–i), with various examples. In most cases, techniques adapted from the semiconductor industry serve as the primary basis for fabrication^{13,28}.

A recent, interesting illustration of the first type of approach is the 'Neuralink' (Fig. 1a) array, where 3,072 sensing sites span across 96 separate soft filaments²⁹, each individually inserted via removable tungsten–rhenium microneedles (24 μm diameter) into rat cerebral cortex. A passive scheme supports channel addressing and thin polyimide coatings serve as encapsulation layers on each filament (20 mm long, 5–50 μm wide, 4–6 μm thick). Coatings of poly(3,4-ethylenedioxythiophene) doped with polystyrene sulfonate (PEDOT:PSS) and iridium oxide (IrO_x) lower the interfacial impedances of the gold electrodes for electrophysiology across sites with areas of $14 \times 24 \mu\text{m}^2$ ($37 \pm 5 \text{ k}\Omega$ for PEDOT:PSS and $57 \pm 7 \text{ k}\Omega$ for IrO_x at 1 kHz). These filaments have potential for chronic use as neural implants due to their ability to move with brain tissues during natural motions associated with respiration and pulsatile blood flow, and to minimize cellular damage and glial scar formation at the biotic/abiotic interface.

Conceptually similar filamentary structures can provide chronic communication with small-diameter nerves. Figure 1b provides an example of electrodes (10–20 μm diameter) formed from multiwalled carbon nanotube (CNT) arrays ($\sim 30 \text{ nm}$ diameter and 250 μm long) for electrical recording in rat glossopharyngeal and vagus nerves³⁰. Here a thin parylene C layer (3.5 μm thick) coats the CNTs except for $\sim 500\text{-}\mu\text{m}$ -long segments at one end, where the yarns wind around a tungsten microneedle for insertion. After removal of the needle, the platform that remains is mechanically compliant (bending stiffness of $\sim 3.3 \times 10^{-12} \text{ Nm}^2$) to motions of the surrounding neural tissues, thereby reducing nerve damage and inflammatory responses. Results include neural recordings in live rat models, where the impedance and signal-to-noise ratio (SNR) remain stable as $18 \pm 8 \text{ k}\Omega$ at 1 kHz and $\sim 10 \text{ dB}$ for up to ten weeks, respectively. Key dimensions and material moduli determine the mechanics based on scaling laws³¹, such that size reduction³² and soft materials³³ can decrease bending stiffnesses and tissue disruption for enhanced stability in operation. For example, miniaturization of filamentary probes yields systems with geometries that can approach those of intrinsic features of neurons themselves (Fig. 1c)³¹. An example, referred to as 'NeuE', consists of 16 recording electrodes (platinum, circular area of $\sim 2 \times 10^2 \mu\text{m}^2$, 50 nm thick) and gold interconnects with substrate/encapsulation layers of a photodefined epoxy polymer (SU-8, 1 μm wide and 0.9 μm thick) that leaves the sensing sites exposed, to yield bending stiffness ($\sim 1.4 \times 10^{-16} \text{ Nm}^2$) comparable to those of individual neurons ($\sim 7.6 \times 10^{-16} \text{ Nm}^2$). These constructs can be injected in a floating form through a syringe into the brains of mice. Interpenetration with neuronal networks allows for multichannel electrophysiological recordings, with stable interfacial impedance ($600 \pm 100 \text{ k}\Omega$ at 1 kHz) and SNR ($\sim 8 \text{ dB}$) for over three months. A key feature of such penetrating probes is their ability to provide cellular and even subcellular level of resolution in measurement and stimulation, with

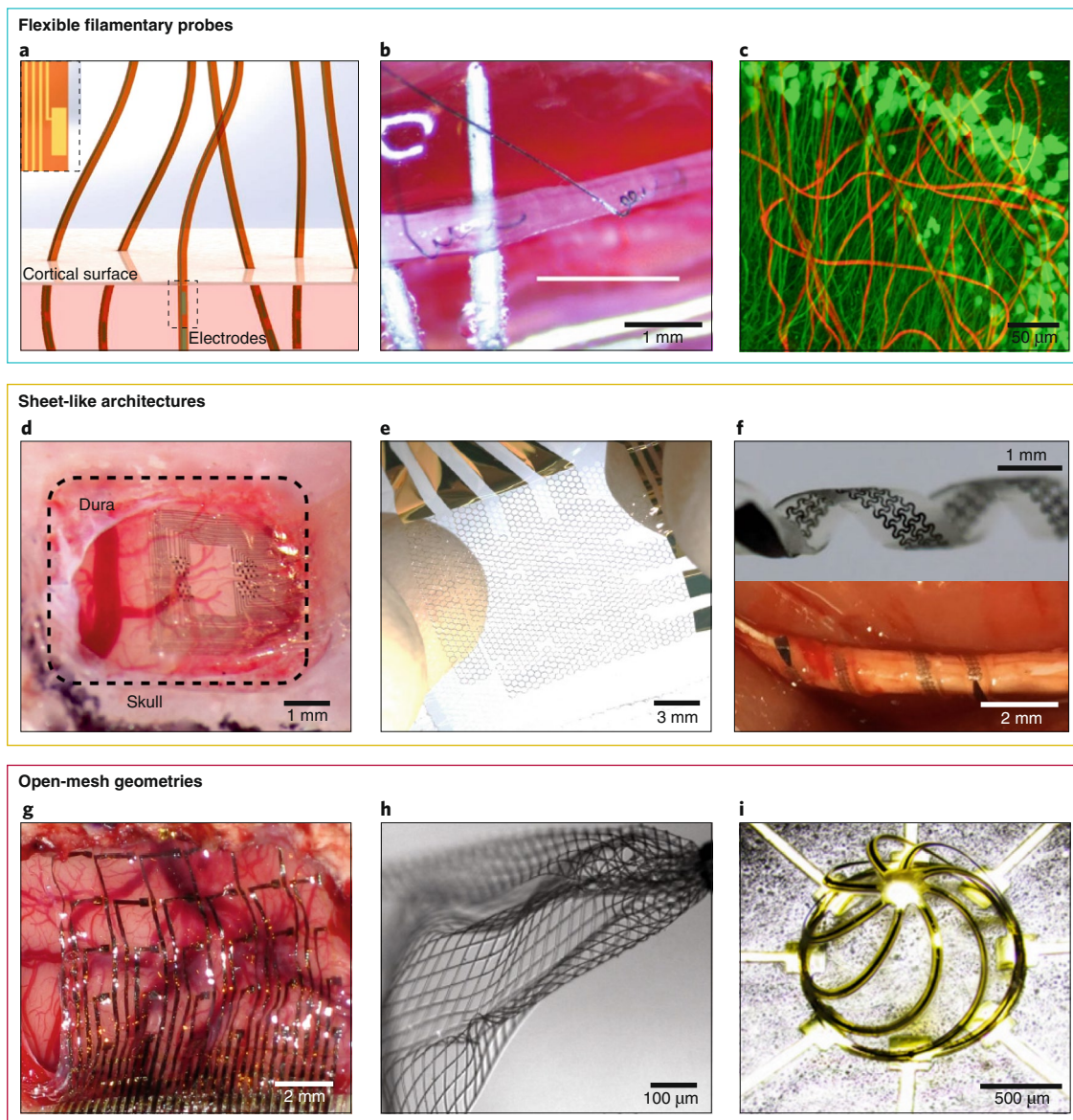


Fig. 1 | Emerging classes of implantable bioelectronic platforms as neural interfaces. **a–c**, Flexible filamentary probes. **a**, Schematic of the surface of rat cerebral cortex with implanted filaments²⁹ (polymer threads, 20 mm long, 5–50 μm wide, 4–6 μm thick), consisting of gold passive electrodes (detail shown in the inset, each area of $14 \times 24 \mu\text{m}^2$). **b**, Optical image of a carbon nanotube yarn (10–20 μm diameter) implanted in the rat vagus nerve, with parylene C layers as encapsulation (3.5 μm thick). **c**, Three-dimensional image of flexible filaments (SU-8, 2–4 μm wide, 0.9 μm thick) that support collections of passive electrodes (platinum, circular area of $\sim 2 \times 10^2 \mu\text{m}^2$, 50 nm thick) (NeuE, red) and neurons (green), two days after implantation in the brain of a mouse. **d–f**, Sheet-like architectures. **d**, Optical image of an array of sensing electrodes (PEDOT:PSS, area of $10 \times 10 \mu\text{m}^2$) embedded in a flexible parylene C sheet (4 μm thick) placed on the rat somatosensory cortex for electrophysiology. **e**, A stretchable OECT array embedded in an ultrathin sheet (parylene diX-SR, 2.6 μm thick) with PEDOT:PSS channels (area of $10 \times 15 \mu\text{m}^2$) while stretched. **f**, Photographs of a soft, stimuli-responsive neural interface (top) capable of conformally wrapping onto peripheral nerves (bottom; 1 mm inner diameter; rabbit model), based on narrow films of polyimide (2 μm thick) with serpentine gold electrodes (200 nm thick) on substrates of a shape-memory polymer ($\sim 100 \mu\text{m}$ thick). **g–i**, Open-mesh geometries. **g**, Photograph of electrode arrays (gold, area of $500 \times 500 \mu\text{m}^2$, 150 nm thick) on ultrathin polyimide mesh (2.5 μm thick) after removal of a bioresorbable silk fibroin substrate, placed on the surface of the brain of a feline animal model. **h**, Optical image of a macroporous open-mesh platform (SU-8, 5–20 μm wide, 1 μm thick) of platinum electrodes (each area of $\sim 1.2 \times 10^3 \mu\text{m}^2$, 50 nm thick), injected into an aqueous bath through a syringe. **i**, Optical image of a three-dimensional scaffold with eight gold electrodes (circular area of $\sim 2 \times 10^3 \mu\text{m}^2$, 300 nm thick) for stimulation and recording, encapsulated by polyimide ($\sim 7 \mu\text{m}$ thick). Panels reproduced with permission from: **b**, ref. ³⁰, Springer Nature Ltd; **c**, ref. ³¹, Springer Nature Ltd; **d**, ref. ³⁴, Springer Nature Ltd; **e**, ref. ³⁵, AAAS; **f**, ref. ³⁷, AAAS; **g**, ref. ³⁹, Springer Nature Ltd; **h**, ref. ⁴⁰, Springer Nature Ltd; **i**, ref. ⁴¹, PNAS.

mechanical compliance matched to brain tissues to minimize the potential for injury.

Ultrathin electrode arrays in sheet-like geometries (at thickness of a few micrometres) exploit related mechanical design principles in flexible surface-mounted systems that can extend over large areas

for recording and stimulating in a non-penetrating fashion, referred to generally as micro-electrocorticography ($\mu\text{-ECoG}$) arrays. An example is shown in Fig. 1d. Here films of PEDOT:PSS serve as the interface material for sensing electrodes (area of $10 \times 10 \mu\text{m}^2$ each) interconnected by patterned metal traces (Pt/Au, $\sim 200 \text{ nm}$ thick)³⁴.

A membrane of parylene C (4 μm thick) provides a substrate/encapsulation layer with sufficient flexibility to conform to the dynamic, curved surfaces of the brain for recording of both local field and action potentials from superficial cortical layers of both rodents and humans. Experiments with such devices span monitoring for patients undergoing epilepsy surgery and operation in rodents over periods of ten days, comparable to requirements for diagnostic recordings in epilepsy patients.

Fully stretchable systems (elastic responses to strains $\gg 1\%$) that can adapt to complex curvilinear and time-dependent biotissue surfaces are also possible, as shown in the 4×4 active multielectrode array of Fig. 1e. Here a layer of parylene diX-SR (Daisan Kasei) formed by chemical vapour deposition (CVD; 2.4 μm thick) and photodefined into an open grid geometry serves both as the encapsulation layer and substrate for organic electrochemical transistors (OECTs; PEDOT:PSS) as the active components (channel area of $10 \times 15 \mu\text{m}^2$ and $\sim 70 \text{ nm}$ thick) and gold as the interconnections³⁵. An outermost layer of an ionically conductive polymer, poly(3-methoxypropyl acrylate) (100 nm thick), offers antithrombotic properties for electrophysiology, as demonstrated in multiplexed electrocardiogram recordings from the cardiac surfaces in live rats. These OECTs provide high transconductances of $\sim 1 \text{ mS}$, roughly 100 times higher than conventional silicon field-effect transistors (FETs)³⁶, leading to recordings with SNRs of $\sim 52 \text{ dB}$. Results demonstrate that such platforms can be stretched reversibly with tensile strains of up to 15%, without degradation in electrical performance. These stretchable OECTs can provide stable transistor characteristics during continuous, complete immersion in phosphate-buffered saline (PBS) for over ten hours, which may be further improved by integrating advanced encapsulation technologies for chronic applications.

Tissue-compliant sheets formed from stimuli-responsive materials are also of interest. Figure 1f shows as an example a climbing-inspired twining system for neural recording and stimulation, based on an array of serpentine electrodes (gold, 200 nm thick) embedded in photodefined strips of polyimide (2 μm thick) on matching substrates of a shape-memory polymer (SMP; $\sim 100 \mu\text{m}$ thick)³⁷. On exposure to physiological conditions (transition temperature of 37 $^\circ\text{C}$) after implantation, these platforms transform from planar geometries into helical structures that spontaneously wrap onto peripheral nerves, with a change in modulus via transition of the SMP from 100 MPa (before transition) to $\sim 300 \text{ kPa}$ (after transition, bending stiffness of $\sim 10^{-10} \text{ Nm}^2$), values comparable to those of neural tissues ($\sim 100\text{--}500 \text{ kPa}$)^{37,38}. In vivo experiments demonstrate capabilities in electrical recording and stimulation of action potentials in rabbit models, with minimized tissue injury during implantation. Current efforts focus on these types of technologies for nerve stimulation, with the potential for use in chronic therapeutic strategies for conditions such as heart failure and epilepsy.

Converting such sheet-like geometries into open-mesh architectures further enhances the mechanics in interconnected arrays, for unique modes of integration with biotissues and cells. Figure 1g illustrates an example of an ultrathin conformal electronic mesh (2.5 μm thick) supported by a bioresorbable substrate of silk fibroin (20–50 μm thick)³⁹. The silk in this case serves as a temporary substrate to facilitate handling; its dissolution yields ultrathin open net-like structures with minimal interface stresses at points of contact with soft biotissues, driven mainly by capillary forces at the biotic/abiotic interface, in forms that can follow complex textures of the surface of the brain. Specifically, these arrays include 30 measurement electrodes (gold, each with an area of $500 \times 500 \mu\text{m}^2$ and 150 nm thick) in a 5×6 configuration with interconnection wires (gold) embedded in a photodefined, thin polyimide mesh (250 μm wide, 2.5 μm thick). In vivo evaluations demonstrate successful mapping of neural processes continuously and without inflammation for more than four weeks on the visual cortex of a feline model.

In other examples, macroporous flexible mesh structures (Fig. 1h)⁴⁰ that incorporate different types of electronic components (platinum electrodes; circular area of $\sim 1.2 \times 10^3 \mu\text{m}^2$, 50 nm thick) or silicon nanowire (Si-NW) FETs and metal interconnects (gold) embedded in photopatterned epoxy encapsulation (5–20 μm wide, $\sim 1 \mu\text{m}$ thick) offer similar mechanics (bending stiffness of $\sim 8.7 \times 10^{-11} \text{ Nm}^2$) with capabilities for delivery through syringe needles (100 μm diameter) using procedures similar to those for the NeuE systems (Fig. 1c). Demonstrations include injection into regions of the hippocampus of live rodents, for neural recordings.

Related classes of open three-dimensional mesostructures but with deterministically controlled layouts can be formed by processes of mechanically induced geometrical transformation from a two-dimensional precursor. The resulting frameworks can serve as active scaffolds for volumetric interfaces to cultured networks of neurons. Figure 1i shows an example in the form of a three-dimensional spherical basket constructed with thin ribbons of polyimide (7 μm thick) that support distributed collections of integrated electrodes (circular gold each with an area of $\sim 2 \times 10^3 \mu\text{m}^2$ and 300 nm thick) for neural sensing and stimulation⁴¹. A nanostructured, biocompatible layer of titanium nitride (50 nm thick) coated onto these gold electrodes increases the interfacial surface area and supports capacitive charge injection during electric stimulation, with high-fidelity capabilities for recording of cellular-action potentials after culturing dorsal root ganglion neurons from rats for seven days. Ongoing efforts with these open-mesh electronics focus on their integration with active components and biocompatible biofluid barriers.

As outlined in Fig. 1, biocompatibility, viewed as a collection of considerations in geometry, mechanics and interface biochemistry that match with targeted biotissues, is essential to stable operation in vivo. The bending stiffnesses associated with the examples in Fig. 1 are many orders of magnitude lower than those of traditional silicon probes (40–100 μm diameter, bending stiffnesses of $\sim 10^{-6} \text{ Nm}^2$)⁴². A key frontier area is in the development of materials for implantable platforms that offer not only these characteristics but also a combination of advanced form factors and distributed high-performance semiconductor functionality. Identifying the proper materials and integrating them together into active bioelectronics platforms with chronic stability represents an exciting area for research, as outlined in various examples that follow.

Long-lasting active systems with biofluid barriers

The existing literature in bioelectronics is largely dominated by systems that rely on passive arrays of electrodes for neural interfaces. Complex functionality such as local signal amplification and active multiplexed addressing demands the integration of semiconductor materials for the required functional components. Examples include platforms that exploit organic transistors on plastic substrates (Fig. 2a), bulk silicon transistors on narrow shanks (Fig. 2b) and Si-NW (Fig. 2c) or Si-nanomembrane (Si-NM; Fig. 2d,e) transistors on sheets or open-mesh structures. The requirements for stable operation depend strongly on the application^{43,44}.

An important focus is on emerging technologies for implants as chronic monitors of neural activity or platforms for neuromodulation, where key material challenges are in permanent implants with operational timescales that can extend to multiple years or decades. In all cases, impermeable barriers to biofluid penetration are essential for isolating the electronics, which are often electrically biased relative to the surroundings, from the adjacent biotissues and fluids while at the same time supporting high-fidelity electrical interfaces. Biocompatible materials for this purpose, in thin-film forms and free of defects over areas that can reach many centimetres square, are critically important for device longevity. As summarized in Fig. 2, much past and current work focuses on organic and/or inorganic coatings and hybrid multilayers formed by spin-casting, physical vapour deposition (PVD) or CVD. Figure 2a provides an example

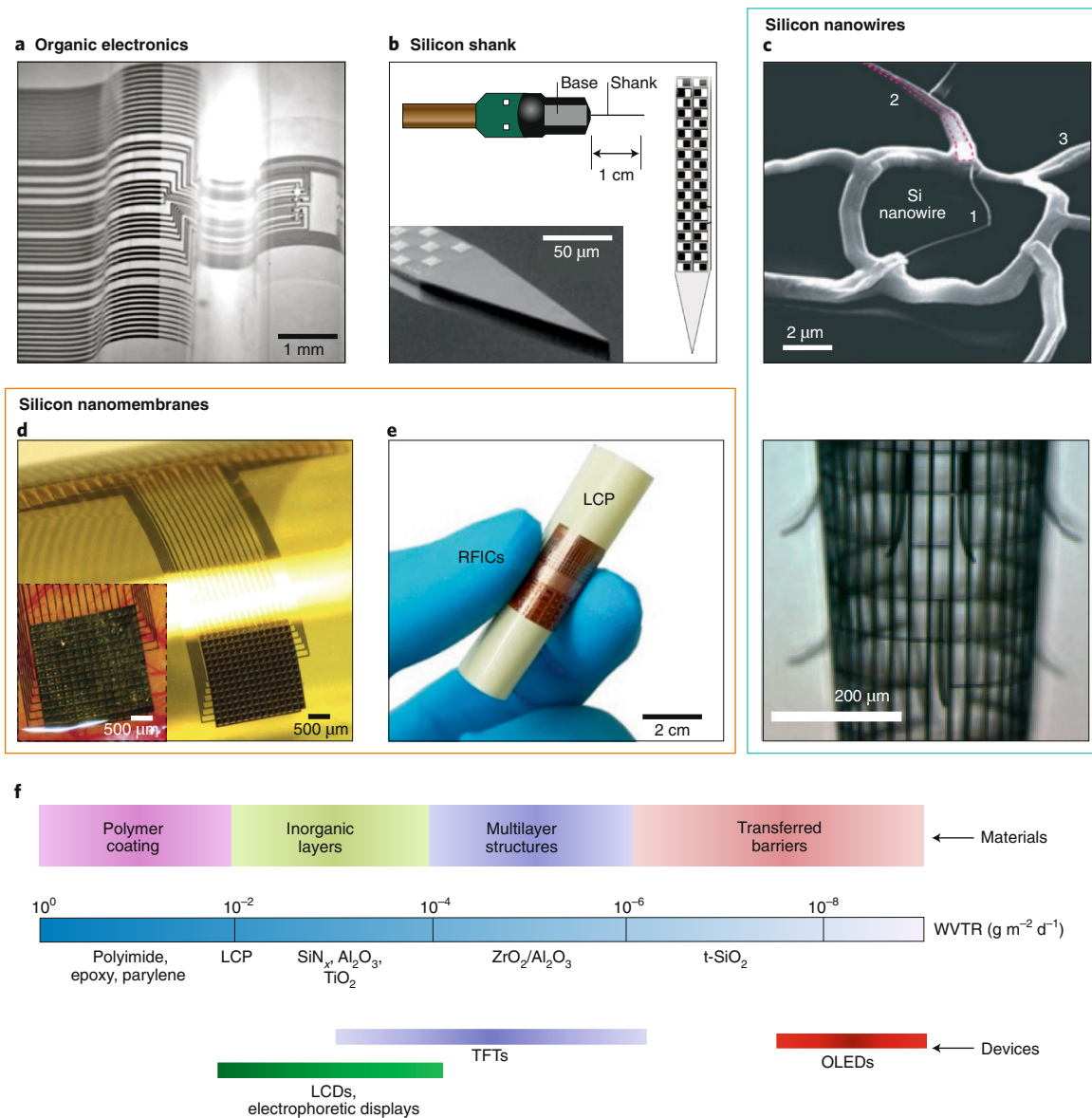


Fig. 2 | Active semiconductor-enabled systems and biofluid barrier materials for device longevity. **a**, Image of a flexible sheet of neural probes on a curvilinear surface, consisting of organic transistors (PEDOT:PSS channel, $6 \times 15 \mu\text{m}^2$ area, 200 nm thick) encapsulated by parylene C (4 μm thick). **b**, Schematic and scanning electron microscope image of a multichannel neural interface system on a rigid shank (left, 1 cm long; cross-sectional dimensions of $70 \times 20 \mu\text{m}^2$). Illustration (right) of the tip of this Neuropixel probe, where the dark squares correspond to titanium nitride recording electrodes (unit size of $12 \times 12 \mu\text{m}^2$, 300 nm thick), encapsulated by SiO₂ (800 nm thick). **c**, Top: scanning electron microscope image of a reticular bioactive scaffold with (1) kinked Si-NW FETs (80 nm diameter), (2) metallic interconnects (Cr/Pd/Cr) and (3) SU-8 encapsulation (1 μm wide, ~1 μm thick). Bottom: micrograph of three-dimensional macroporous networks as brain probes with polymer encapsulation (SU-8, 7 μm wide, 1 μm thick) and Si-NW FETs distributed at each supporting arm. **d**, Photograph of an actively multiplexed array of Si-NM transistors (unit size of $200 \times 200 \mu\text{m}^2$) on a polyimide substrate (12.5 μm thick), placed on a curved glass surface, encapsulated by multilayers of polyimide (~2.4 μm thick) and epoxy (4 μm thick). The inset shows the array in contact with the auditory cortex of a rat. **e**, Photograph of flexible Si-NM radio-frequency-integrated circuits (RFICs) supported by layers of LCP (50 μm thick) in a bent state. **f**, Schematic of approximate ranges of WVTRs (at 25 °C, 100% RH) for various barrier materials with requirements for different types of common flexible devices, including organic light-emitting devices (OLEDs), thin-film transistors (TFTs), liquid crystal displays (LCDs) and others. Panels reproduced with permission from: **a**, ref. ⁴⁵, Springer Nature Ltd; **b**, ref. ⁴⁷, Springer Nature Ltd; **c**, top, ref. ⁴⁹, Springer Nature Ltd; bottom, ref. ⁵⁰, Springer Nature Ltd; **d**, ref. ⁵², American Physiological Society; **e**, ref. ⁵³, American Chemical Society; **f**, ref. ⁵⁶, Elsevier.

of a flexible system of OECTs designed to record electrophysiological signals on the surface of the rat brain⁴⁵. Here the transistors lie beneath sheets (4 μm thick) of parylene C formed by CVD, with photopatterned openings to expose the channel regions of the transistors (PEDOT:PSS, channel area of $6 \times 15 \mu\text{m}^2$ and 200 nm thick) as biocompatible sensing interfaces. These active polymer electrodes enable electrophysiological recordings of low-amplitude

epileptiform discharges by local amplification, with stable electrical performance⁴⁶. Results of soak tests demonstrate stability during immersion in cell culture media (Dulbecco's modified Eagle medium (DMEM)) at 37 °C over five weeks.⁴⁵ An important feature of these OECTs is that the electronics themselves, not just the electrodes, integrate directly with targeted biotissues. The resulting functionality cannot be reproduced by passive devices, where

capabilities for local signal amplification and multiplexed addressing follow naturally. Although the lifetime of passive electrodes can be long due to the relatively low sensitivity to leakage currents, active systems represent the current frontier of bioelectronics research.

Compared with organic electronic materials, inorganic semiconductors and associated processing approaches adapted from the integrated circuit industry can offer advantages in functionality and performance. As an example, Fig. 2b highlights the use of silicon technology as the basis for penetrating probes⁴⁷ that support dense arrays of 960 sensing/stimulation sites with integrated complementary-metal-oxide-semiconductor (CMOS) circuits distributed along a rigid shank (1 cm long; cross-sectional dimensions of $70 \times 20 \mu\text{m}^2$). The designs of such probes minimize damage to brain tissues, compared with more well-established silicon needle arrays (10×10 , each with $100 \mu\text{m}$ diameter)¹³. The CMOS supports multiplexed addressing and local amplification at each recording site. Layers of SiO_2 (plasma-enhanced CVD, 800 nm thick) serve as biofluid barriers with openings at the measurement sites⁴⁸, where titanium nitride electrodes (area of $12 \times 12 \mu\text{m}^2$ for each site and ~ 300 nm thick) form low-impedance electrical interfaces (dark squares in Fig. 2b, $\sim 149 \pm 6$ k Ω at 1 kHz). High-density recordings of over 700 isolated neurons across deep regions of brain at a depth of ~ 4 mm beneath the primary cortex (which include the visual cortex, hippocampus, thalamus, motor cortex and striatum) are possible, with stable operation for up to 150 days in mouse models. Although these types of systems offer capabilities for neural recordings in deep-brain structures, their rigid construction and planar designs preclude their use in large two-dimensional arrays or extended three-dimensional networks.

Penetrating probe technologies that exploit inorganic systems and barrier strategies but with additional features in spatially extended geometries and with mechanical compliance are of growing interest. Figure 2c (top) shows an example of a flexible bioactive mesh, consisting of kinked Si-NW FETs (80 nm diameter), metallic interconnects (Cr/Pd/Cr) and photopatterned epoxy encapsulation (spin-cast SU-8, 1 μm wide and $\sim 1 \mu\text{m}$ thick). Studies show that these nanowire platforms can integrate as reticular cellular scaffolds for culture of neurons from rats⁴⁹, where the FETs remain stable for nine weeks. Scaling of such concepts to platforms with 60 interconnected FETs distributed across a mesh area of $\sim 3.5 \times 1.5 \text{ cm}^2$ (bending stiffness $\sim 6 \times 10^{-12}$ – $1.3 \times 10^{-9} \text{ Nm}^2$) yields capabilities in real-time multiplexed monitoring and recording of the electrical activity within the scaffold/neuron system. Recent efforts on these types of systems include integration of tissue-compliant arrays with biotissues in a penetrating fashion in animal models. A temporary support provides mechanical stability during insertion and is subsequently removed.

Similar macroporous networks can be formed into three-dimensional global penetrating probes with additional advantages (Fig. 2c, bottom)⁵⁰. Reported examples incorporate 13 Si-NW FETs at each supporting arm of systems that bend outwards from the cylinder surface to serve as multiplexed sensors for neural signals, with metallic interconnects (Cr/Pd/Cr) encapsulated in thin photodefined layers of epoxy (SU-8, 5 μm wide and 1 μm thick). Such flexible platforms can be temporarily rigidified by immersion in liquid nitrogen, to allow insertion into rodent brains at a depth of ~ 1.5 mm for subsequent electrical recording and stimulation of local field potentials from a subregion of the barrel cortex. The ultralow bending stiffness ($\sim 0.64 \times 10^{-15} \text{ Nm}^2$) promotes gentle, conformal tissue contacts with minimal mechanical perturbation, many orders of magnitude lower than those of silicon probes ($\sim 10^{-9} \text{ Nm}^2$, cross-sectional area of $15 \times 60 \mu\text{m}^2$)²⁵. Critical challenges of these Si-NW-based systems include limited numbers of channels and challenges in scalability as well as relatively short operational lifetimes (typically days or weeks). Further developments may enable high-density mapping of neural activity, with optimized schemes for integration with targeted tissues⁵¹.

Devices with alternative forms include thin, flexible sheets designed to allow for large-area interfaces to the soft, dynamic surface of the brain in a non-penetrating manner. Some of most sophisticated systems support $\sim 10^3$ Si-NM transistors per centimetre square, with amplified and multiplexed channels for electrophysiological mapping on cortical or epicardial surfaces^{21,22}. Figure 2d shows an example of a two-dimensional array of interconnected Si-NM transistors as an electronic backplane on a thin polyimide film ($\sim 13 \mu\text{m}$ thick), coated with multilayers of polyimide/epoxy (2.4/4.0 μm thick) photolithographically patterned to define openings at platinum electrodes (50 nm thick) that connect to the transistors⁵². Related reports present exploded-view schematics of such active, multichannel systems, with layer configurations and barrier materials²². Examples of scalable application of such concepts to high-channel-count systems with active components include 196-channel arrays (14×14 configuration, unit size of $200 \times 200 \mu\text{m}^2$, resolution of $250 \mu\text{m}$) consisting of 392 transistors distributed across areas of $\sim 12 \text{ mm}^2$ ($\sim 25 \mu\text{m}$ thick) for auditory-cortex recordings in rats⁵², 288-channel arrays of amplified electrodes (18×16 configuration, unit size of $250 \times 250 \mu\text{m}^2$, resolution of $800 \mu\text{m}$) with 2,016 transistors and areas of $\sim 180 \text{ mm}^2$ ($\sim 48 \mu\text{m}$ thick) for cardiac electrophysiology in porcine models²¹, and 360-channel electrode arrays (18×20 configuration, unit size of $300 \times 300 \mu\text{m}^2$, resolution of $500 \mu\text{m}$) with 720 transistors and areas of $\sim 90 \text{ mm}^2$ ($\sim 25 \mu\text{m}$ thick) for visual-cortex recordings in feline models²². These types of technologies offer lifetimes in vivo that are typically measured in weeks or months, limited mainly by water penetration through polymeric barrier layers as the key limitation for chronic use.

Flexible materials that can serve as superior alternatives to polyimide, epoxy, parylene and other traditional polymeric biofluid barriers are required for long-term, stable operation in biofluids. An example is in Fig. 2e, where pre-formed sheets of liquid crystal polymer (LCP, 50 μm thick) bond on both the top and bottom sides of Si-NM-based radio-frequency-integrated circuits, as barriers in an envisioned in vivo wireless network of subcutaneous implants in live rats⁵³. LCP materials have low rates of water permeation, and in this example, projections based on soak tests in PBS solution at elevated temperatures suggest lifetimes in vivo of up to about two years. The relatively thick geometry, however, limits the flexibility of system and heavily constrains options in the design of the electrical biointerface for sensing and stimulation.

Attractive features in neural interfaces include tissue-compliant mechanics and surface mounting configurations to minimize tissue damage (Fig. 2a), active bioelectronic components (Fig. 2d,e) and microscale, penetrating features (Fig. 2b,c) for recordings at depths below the surface. Recent research indicates that silicon-membrane diodes (1.25 μm thick) can serve as penetrating probes embedded in polyimide shanks (~ 1.5 mm long, 6 μm thick) and distributed on a conformal sheet (polyimide, 6 μm thick). These diodes act as photodetectors for mapping light intensity, with potential in neural optogenetic applications⁵⁴. Additional work may establish means for increasing the density of such penetrating probes, possibly with advanced active electronics (such as multiplexed transistor array) for chronic operation.

Table 1 summarizes the mechanical properties and types/functions of constituent materials for all cases outlined in Figs. 1 and 2, where the bending stiffnesses of various systems ranges from $\sim 1.4 \times 10^{-16}$ to $1.0 \times 10^{-10} \text{ Nm}^2$ and the operational lifetimes during implantation are typically in the range of months. An ambitious goal is to combine active electronic and/or optoelectronic functionality with water-impermeable barrier materials that can establish gentle, conformal interfaces to biotissues and offer stable operation for long-term lifetime (up to decades or more).

To compare different materials as biofluid barriers, the water vapour transmission rate (WVTR, with units of $\text{g m}^{-2} \text{ d}^{-1}$, sometimes referred to the water permeation rate)⁵⁵, a widely used and

Table 1 | Summary of key materials used in the various device platforms of Figs. 1 and 2

Studies	Subject	Key materials	Thickness (μm)	Bending stiffness (Nm^2)	Functions	Operational lifetime <i>in vivo</i> ^a
Ref. ²⁹	Rat	Polyimide/gold	4–6	–	Recording/stimulation	–
Ref. ³⁰	Rat	Parylene/CNT	3.5	3.3×10^{-12}	Recording/stimulation	10 weeks
Ref. ³¹	Mouse	Epoxy/platinum	0.9	1.4×10^{-16}	Recording	3 months
Ref. ³⁴	Rodent	Parylene/PEDOT:PSS	4	–	Recording	10 days
Ref. ³⁵	Rat	Parylene/PEDOT:PSS	2.6	–	Recording	–
Ref. ³⁷	Rabbit	Polyimide/gold/SMP	~100	1.0×10^{-10}	Recording/stimulation	–
Ref. ³⁹	Feline	Polyimide/gold	2.5	–	Recording	4 weeks
Ref. ⁴⁰	Rodent	Epoxy/platinum	1	8.7×10^{-11}	Recording	–
Ref. ⁴¹	Rat	Polyimide/gold	7	–	Recording/stimulation	–
Ref. ⁴⁵	Rat	Parylene/PEDOT:PSS	4	–	Recording	–
Ref. ⁴⁷	Rat	SiO ₂ /titanium nitride	20	–	Recording	153 days
Ref. ⁴⁹	Rat	Epoxy/Si-NW	1	6.2×10^{-12}	Recording/stimulation	–
Ref. ⁵⁰	Rat	Epoxy/Si-NW	1	0.64×10^{-15}	Recording/stimulation	–
Ref. ⁵²	Rat	Epoxy/Si-NM	~20	–	Recording	–
Ref. ⁵³	Rat	LCP/Si-NM	50	–	RFID	6 weeks

Constituent materials involve CNTs, SMPs, Si-NWs and Si-NMs, with system functions that include recording, stimulation and radio-frequency identification (RFID). ^aOperational lifetimes *in vivo* refer to the experimental timescales demonstrated in animal models in each case.

well-established parameter for encapsulation in many different conventional classes of devices and products, can serve as an indirect but valuable comparative metric for initial assessment of possibilities⁵⁶, often expressed as $\text{WVTR} = D_{\text{eff}}(C_1 - C_2)/l$, where D_{eff} is the effective diffusion coefficient of the barrier material, l is the thickness and C_1 and C_2 are the water concentrations at the front and back sides of the barrier layer⁵⁷. Permeation generally involves a diffusion process (both liquid and vapour) through the barrier materials starting at the front side during immersion in biofluids or within a high-humidity environment, where the difference is that the initial water concentration (C_1) for the former (immersion, $\sim 1 \text{ g cm}^{-3}$) is many orders of magnitude higher than that of the latter (100% relative humidity (RH), $\sim 10^{-4} \text{ g cm}^{-3}$).

Figure 2f summarizes literature results at a specific condition (25 °C, 100% RH) along with approximate ranges that define requirements for different types of flexible devices. Previous work on encapsulation for displays that use organic light-emitting diodes has some relevance for the topic of this Review. Polymers (such as SU-8, polyimide and parylene) and deposited inorganic materials (such as SiN_x and Al₂O₃) generally fail to offer sufficient water-barrier properties, where WVTR values range from 10^2 to $10^{-2} \text{ g m}^{-2} \text{ d}^{-1}$ (refs. ^{56,58,59}) and from 10^{-2} to $10^{-4} \text{ g m}^{-2} \text{ d}^{-1}$, respectively^{58,60}. The limits for the former follow from the intrinsic permeability associated with the free volume of the polymer, the sizes of mobile chains and the interactions between the polymer and the biofluids⁶¹, all of which affect the diffusion of water through the polymer under specific conditions⁵⁷. Here the effective water diffusion coefficient (D_{eff} , unit of $\text{cm}^2 \text{ s}^{-1}$) can serve as a key property to compare various barrier structures. For a given polymer, increasing the density tends to decrease the free volume and therefore lower the diffusivity; hydrophobic chemical groups and efficient chain packing can also lead to decreases⁶². For example, elastomers such as silicones have high D_{eff} values ($\sim 10^{-6} \text{ cm}^2 \text{ s}^{-1}$ at $\sim 35 \text{ °C}$)⁶³ while parylene C and LCPs offer comparatively low values (10^{-11} to $10^{-9} \text{ cm}^2 \text{ s}^{-1}$ at room temperature) due to differences in density, free volume and optimized chain packing within crystalline structures^{62,64}. Of note is that LCP layers based on previous studies typically involve thick geometries (50–500 μm thick)^{53,59}, thereby leading to low WVTR

values ($\sim 10^{-3} \text{ g m}^{-2} \text{ d}^{-1}$) compared with those typically quoted for other types of polymers.

Inorganic barrier materials formed as films by techniques such as atomic-layer deposition (ALD) or CVD offer superior properties compared with those of organics, with D_{eff} values that can be as low as $\sim 10^{-13} \text{ cm}^2 \text{ s}^{-1}$ for the case of ALD TiO₂ at 60 °C (ref. ⁶⁵) and $\sim 10^{-16} \text{ cm}^2 \text{ s}^{-1}$ for CVD SiO₂ at 40 °C (ref. ⁶⁶), with correspondingly low values for the WVTR (as in Fig. 2f). Nevertheless, extrinsic imperfections associated with deposition or growth, such as micro-/nanocracks, pinholes, grain boundaries, incomplete coverage and other defects, can be nearly impossible to eliminate, especially when formed in academic cleanroom facilities on surfaces that present disparate surface chemistries and challenging topography. The most common means to enhance the barrier performance features alternating multilayer structures of organic and inorganic materials, or inorganic materials alone. ALD can yield materials (such as Al₂O₃, HfO₂, ZrO₂) in multilayer structures with thin geometries ($\sim 100 \text{ nm}$ thick) at low deposition temperatures ($\sim 100 \text{ °C}$), as often used in organic light-emitting device displays⁵⁷, where the WVTR can range from 10^{-3} to $10^{-5} \text{ g m}^{-2} \text{ d}^{-1}$. As an example, a repeating structure of Al₂O₃/ZrO₂ (2.6 nm/3.6 nm, total $\sim 130 \text{ nm}$ thick) offers superior barrier performance (WVTR of $\sim 4.7 \times 10^{-5} \text{ g m}^{-2} \text{ d}^{-1}$ at 70 °C, 70% RH) compared with those of other types of multilayer combinations^{67,68}. Here a stable phase of ZrAl₃O₇ forms at the Al₂O₃/ZrO₂ interface. Increasing numbers of material interfaces increases the permeation paths for water diffusion, yielding enhancements in relevant barrier performance⁶⁷.

Challenges in these and related types of schemes are not only in reliably forming such coatings on pre-fabricated devices, with levels of materials heterogeneity and surface topography mentioned previously, but also in overcoming the limitations associated with processing conditions (chemistries, plasma exposures, temperatures) that must be compatible with the underlying bioelectronics. Schemes that circumvent these constraints decouple the device and its fabrication from synthesis and deposition procedures to define the biofluid barrier⁶⁹. Here optimized conditions yield barrier layers of the best choices of materials on temporary substrates (such as polished silicon wafers), configured to minimize the potential

for formation of defects, independent of any other considerations. Subsequent steps then yield patterned layers of active and passive materials for functional bioelectronics systems on the surface of the barrier layer. Bonding to a substrate of interest (such as flexible plastic sheet) and eliminating the temporary substrate completes the process (referred to an inverted fabrication sequence), where the bottom surface of the barrier layer now forms the biointerface. Other schemes involve physical transfer of the barrier, pre-formed in this manner (referred to as a transferred barrier, Fig. 2f), onto a completed bioelectronic device. The advantages include formation of the encapsulation layer using optimized conditions (such as high deposition/annealing temperatures, pressures, chemical/plasma exposures and substrate surfaces/chemistries) without constraints associated with other materials or device structures and broad applicability across a wide range of material types for the barrier and the electronics⁵³.

Approaches for chronically stable materials and devices

Recent efforts to develop multichannel electrical neural interfaces focus on chronically stable materials approaches and device designs that provide multiplexed signal readout and per-channel amplification in a way that avoids cross-talk between neighbouring channels, of particular importance in systems with thousands of channels⁷⁰. Here the key features are the barrier layers, which often serve not only as robust encapsulation structures in thin, flexible forms but also as high-quality electrical interfaces to surrounding biotissues. The best cases offer high-fidelity operation with projected lifetimes of multiple decades. Recent reports describe the use of physically transferred layers of SiO₂ thermally grown on surfaces of device-grade silicon wafers as key components of high-performance bioelectronic systems (Fig. 3a) that offer unmatched operating lifetimes for active, flexible devices in simulated biofluids and in live animal models⁶⁹. The nature of the growth process (thermal oxidation, ~1,150 °C) yields dense, uniform and defect-free layers of SiO₂ (referred as t-SiO₂) with highly controlled thicknesses, typically in the submicrometre range. The resulting materials offer exceptional barrier performance, in a biocompatible class of material with excellent mechanical compliance by consequence of the thin geometry. The WVTR (~10⁻⁶–10⁻⁸ g m⁻² d⁻¹ with a thickness of 1 μm, at 25 °C, 100% RH) of t-SiO₂ is considerably higher than layers of SiO₂ formed by other methods (CVD, ALD, sol-gel processing)^{71–73}, and the growth-based strategy on silicon wafers leads to films that are essentially free of defects, even in the environments with limited particulate and chemical control such as those found in most academic cleanrooms. Mechanical grinding and dry etching processes remove the wafer following the inverted fabrication sequence or before physical transfer. Depending on requirements, an additional transfer step can deliver a similar barrier layer onto the opposite side of a completed system. Examples of t-SiO₂ for encapsulation of bioelectronic systems in this fashion focus on capacitively coupled devices, with active multiplexing and local buffering by arrays of Si-NM transistors, as described in detail in the following⁶⁹.

Figure 3a schematically illustrates capacitive coupling to an electrode (gold pad, 270 × 460 μm²) that connects to an underlying Si-NM transistor. Here, the t-SiO₂ layer (900 nm thick) serves not only as the biofluid barrier but also as the capacitive interface to the adjacent biotissues, such that associated biopotentials modulate the channel of the Si-NM transistor. An optical micrograph of a representative unit cell in a flexible, actively multiplexed array (18 rows, 22 columns) for cardiac electrophysiological mapping is shown in Fig. 3a (right). Each cell includes two Si-NM transistors: one for multiplexing and one for amplification⁶⁹. Such coupling mechanisms offer signal amplification and minimize cross-talk. In vitro tests involve complete immersion in PBS solution (pH 7.4) at different temperatures. In all cases, a slow hydrolysis process

(SiO₂ + 2H₂O → Si(OH)₄) that proceeds by surface erosion represents the only factor that limits the lifetime, as opposed to extrinsic and intrinsic effects associated with pinhole defects or water permeation, respectively. Temperature-dependent measurements of the rates of hydrolysis of t-SiO₂ in PBS appear in Fig. 3b, at temperatures *T* of 27 °C, 37 °C, 50 °C, 70 °C and 90 °C, via assessments of thickness using ellipsometry. The results show a linear relationship between these rates and 1/*T*, consistent with Arrhenius scaling⁷⁴. The data indicate an activation energy of *E*_A = 1.32 eV, corresponding to an exceptionally slow rate of change in thickness at 37 °C (~15 nm yr⁻¹)⁷⁴. This result suggests operational timeframes of systems encapsulated with t-SiO₂ layers that can extend to the life of patient (>70 years at a thickness of ~1 μm).

Although promising as water barriers, species of ions present in biofluids, such as sodium (Na⁺), can diffuse through t-SiO₂ layers under applied bias (*V*_{app}) as a driving force, because t-SiO₂ has a high ion diffusivity (6.53 × 10⁻¹⁷ cm² s⁻¹ at 37 °C) compared with those of other materials such as CVD SiN_x (~4.94 × 10⁻²¹ cm² s⁻¹)⁷⁵. Figure 3c shows numerical simulations for the spatial distribution of Na⁺ through the thickness of the t-SiO₂ (1 μm thick) along with the corresponding electrostatic potential profile for various *V*_{app} and immersion in 96 °C PBS for ten days⁷⁵, in an ideal situation and without considering the dissolution of t-SiO₂. The Na⁺, driven by different *V*_{app}, penetrates through the t-SiO₂ layer and accumulates at the interface with the underlying silicon substrate. This process can degrade the performance of the electronics by shifting the threshold voltages of the transistors. Addition of capping layers on top of the t-SiO₂ can prevent the diffusion of ions⁷⁶. Secondary-ion-mass-spectroscopy data reveal ion-concentration profiles in the t-SiO₂ (100 nm thick) in isolation and as integrated into a trilayer structure (polyene C/HfO₂/t-SiO₂, 50/50/100 nm thick), as a function of depth under different *V*_{app} (0 V, 3 V) (Fig. 3d). The trilayer decreases the concentration of Na⁺ at the surface of the Si by a factor of ~10³ for *V*_{app} = 3 V after immersion for two days in 37 °C PBS. In addition to blocking ion diffusion, immersion tests demonstrate that the capping layers (polyene C/HfO₂, 50/50 nm thick) also slow the dissolution of the underlying t-SiO₂ in simulated biofluids at different elevated temperatures. Extrapolation of the results yield projected rates of ~10⁻⁴ nm d⁻¹ and ~0.04 nm d⁻¹ in 37 °C PBS for cases with and without the capping layers, respectively^{74,76}, thereby establishing a simple scheme for enhancing the expected lifetimes.

One inherent limitation of this type of approach is that the barrier is unpatterned and its highly insulating properties impose limits on options in sensing and stimulation due to the associated high impedance (t-SiO₂, 900 nm thick, ~2.6 GΩ at 10 Hz)⁶⁹. Specifically, because sensing occurs by capacitive coupling, design layouts favour either large sensing areas or thin geometries in the t-SiO₂ to achieve high coupling capacitance and low-noise operation. Scaling of either type degrades performance by compromising spatial resolution (large sensing areas) and system lifetimes (thin barrier thicknesses). Recent reports describe a solution that combines highly doped silicon Si-NMs (p⁺⁺-Si, ~10²⁰ cm⁻³, boron dopants) monolithically bonded to t-SiO₂ (ref. 77). Here, as illustrated in Fig. 3e, dry and wet etching procedures define small openings through a layer of t-SiO₂ (area of 15 × 15 μm²) to expose an underlying p⁺⁺-Si-NM at each unit cell, all created from the device silicon layer and the buried oxide of a silicon-on-insulator wafer following removal of the handle wafer. The result is a conducting via structure integrated with the layer of t-SiO₂, which we refer to as p⁺⁺-Si//t-SiO₂, where the p⁺⁺-Si serves as both a biofluid barrier and a direct, conductive electrical interface that connects an underlying backplane of electronics built around Si-NM transistors to targeted biotissues. Figure 3e (right) presents an optical image of a unit cell of this type in an actively multiplexed array (64 channels, 8 rows, 8 columns) designed for neural recording. Here, thin-film electrodes

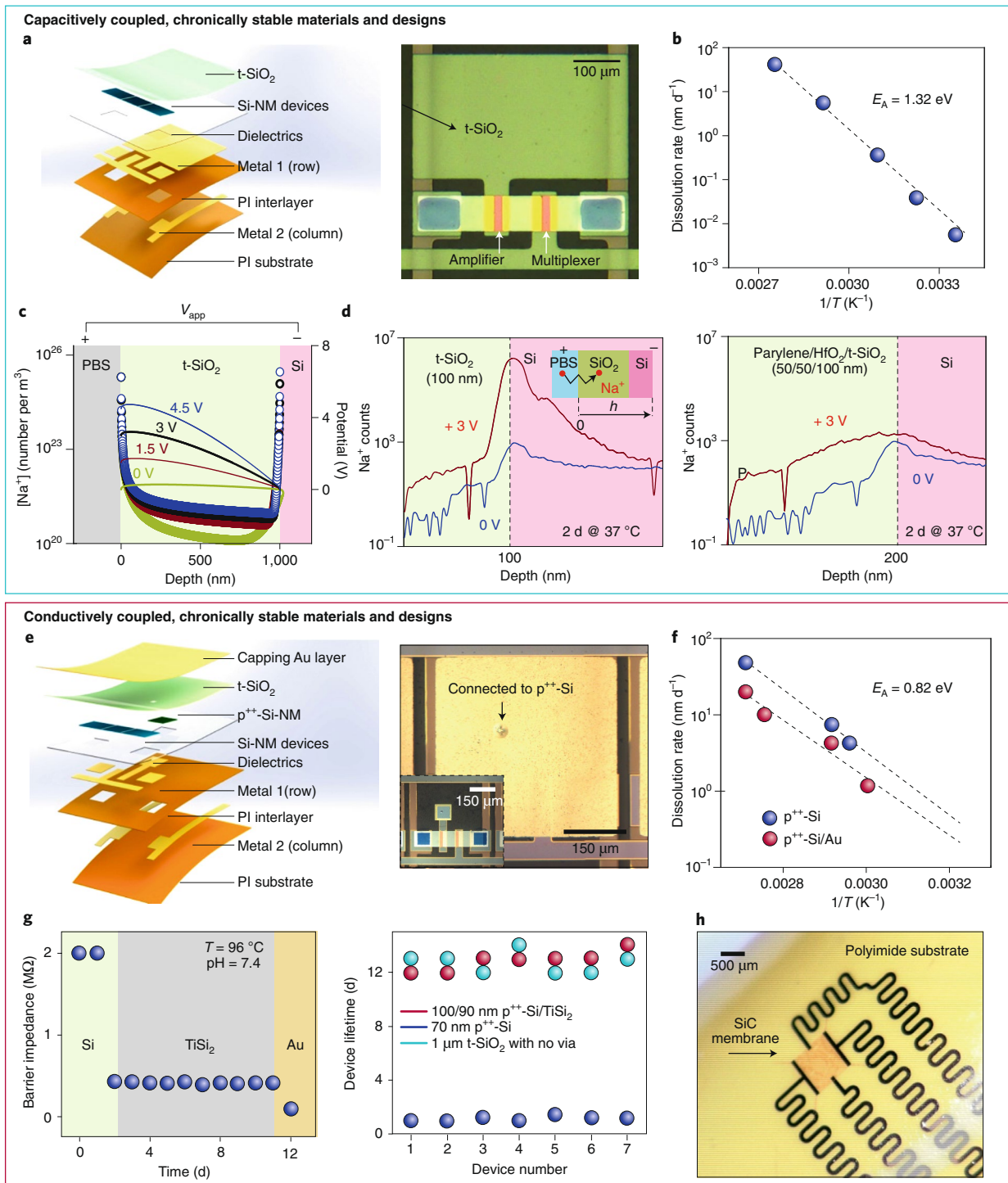


Fig. 3 | Materials and engineering approaches for chronically stable, active electronic neural interfaces. **a**, Left: mechanism for capacitively coupled sensing through a layer of t-SiO₂ to an Si-NM transistor on polyimide (PI). Right: image of a unit cell with a layer of t-SiO₂ as encapsulation. **b**, Dissolution rate of t-SiO₂ in PBS at different temperatures, at pH of 7.4. **c**, Concentration of Na⁺ ([Na⁺]) and potential distributions in t-SiO₂ for V_{app} between a Pt probe in PBS and transistor electrodes, after immersion for 10 days in PBS (96 °C). **d**, Cross-sectional profile of [Na⁺] under different V_{app} with a layer of t-SiO₂ (left) and with a trilayer of parylene/HfO₂/t-SiO₂ (right) after immersion for 2 days in 37 °C PBS. The inset is an illustration of the geometry, where *h* is the thickness. **e**, Left: mechanism for conductively coupled sensing through a hermetic-via structure (p⁺-Si/t-SiO₂) to a Si-NM transistor. Right: image of a unit cell before (inset) and after deposition of a capping layer of Au, encapsulated by Au/p⁺-Si/t-SiO₂. **f**, In vitro tests of dissolution of p⁺-Si with and without an Au coating in PBS at different temperatures. **g**, Left: change of barrier impedance as a function of time at 1 kHz during soak test in PBS at 96 °C. Right: comparison of lifetimes of devices with p⁺-Si/TiSi₂/t-SiO₂, p⁺-Si and t-SiO₂ barrier designs. **h**, Flexible bio-integrated electronics based on a layer of monocrystalline SiC on a polyimide substrate, wrapped around a curved surface. Panels reproduced with permission from: **a**, ref. ⁶⁹, Springer Nature Ltd; **b**, ref. ⁷⁴, PNAS; **c**, ref. ⁷⁵, Wiley; **d**, ref. ⁷⁶, American Chemical Society; **e, f**, ref. ⁷⁷, PNAS; **g**, ref. ⁷⁹, American Chemical Society; **h**, ref. ⁸³, American Chemical Society.

(gold, 300 nm thick) on top of p^{++} -Si/ t -SiO₂ act as the conductively coupled interface that covers the entire area of each unit cell (area of $360 \times 360 \mu\text{m}^2$), for fill factors that can approach $\sim 100\%$ (ratio of the area of the sensing/stimulation electrode to the area of the unit cell) with p^{++} -Si-NMs that consume only a small fraction of the corresponding area for the electronics ($\sim 5\%$ fill factor). This construction also forms a bilayer barrier of p^{++} -Si (device side, 60 nm thick)/Au (biotissue side, 300 nm thick) to improve system lifetimes. The results of soak tests for barrier designs with and without gold films are shown in Fig. 3f, with experimental measurements of dissolution rates of p^{++} -Si layers ($\text{Si} + 4\text{H}_2\text{O} \rightarrow \text{Si}(\text{OH})_4 + 2\text{H}_2$). The rate can be reduced to $\sim 20 \text{ nm d}^{-1}$ with a capping layer of gold (300 nm thick) in 96 °C PBS (compared with $\sim 50 \text{ nm d}^{-1}$ without the gold), with an activation energy of $E_A = 0.82 \text{ eV}$ (ref. 77). On the basis of the linear relationship between rates and $1/T$ in Arrhenius scaling, a projected dissolution rate of $\sim 0.2 \text{ nm d}^{-1}$ in 37 °C PBS can lead to a lifetime of about one year.

A further enhancement of this general approach replaces the p^{++} -Si, which has a rate of dissolution that is high compared with that of t -SiO₂ (p^{++} -Si: ~ 0.5 – 4.0 nm d^{-1} depending on ionic concentration, in 37 °C PBS, 10^{20} cm^{-3} dopants; t -SiO₂: $\sim 0.04 \text{ nm d}^{-1}$)^{74,77,78} with titanium silicide (TiSi₂) derived by thermal annealing (at 850 °C) of titanium deposited on a Si-NM (p^{++} -Si) on t -SiO₂ (ref. 79). The resulting bilayer structure of p^{++} -Si/TiSi₂, exposed through openings etched in the t -SiO₂, can serve as encapsulation and bio-interface, which we refer to as p^{++} -Si/TiSi₂/ t -SiO₂. Figure 3g (left) shows the time evolution of the impedance at 1 kHz associated with multilayer constituent materials (p^{++} -Si (100 nm)/TiSi₂ (90 nm)/ t -SiO₂ (1 μm)) on a gold pad (50 μm diameter, 300 nm thick) during immersion in 96 °C PBS. During the soak tests, degradation of the barrier begins with dissolution of the top p^{++} -Si at a rate of $\sim 50 \text{ nm d}^{-1}$ in PBS at 96 °C, indicating that the impedance remains at $\sim 500 \text{ k}\Omega$ after exposure of underlying TiSi₂ (day 2). The TiSi₂ remains functional (days 3–11) until complete dissolution of the surrounding t -SiO₂, which occurs at a rate of $\sim 90 \text{ nm d}^{-1}$ under similar conditions⁷⁴. The t -SiO₂ (1 μm thick) disappears after 12 days, without any measurable change in the thickness of the TiSi₂ layer, resulting in lateral water penetration to the gold pads and a corresponding dramatic decrease in the impedance. These results suggest a survivability of the structure (p^{++} -Si/TiSi₂, 100/90 nm thick) that is superior to that of t -SiO₂ (~ 70 years at 1 μm thickness in 37 °C PBS). Comparisons of lifetimes of Si-NM transistors in 96 °C PBS based on different encapsulation strategies (t -SiO₂, p^{++} -Si and p^{++} -Si/TiSi₂/ t -SiO₂) with various thicknesses appear in Fig. 3g (right), with an emphasis on the chronic stability of p^{++} -Si/TiSi₂/ t -SiO₂ (100 nm/90 nm/1 μm thick), comparable to that of a single t -SiO₂ layer (1 μm thick). The data indicate that in these materials systems, the lifetime is only limited by hydrolysis of t -SiO₂. Specifically, because the material does not react with water, the TiSi₂ layer provides a water diffusion rate of $\sim 3 \text{ nm d}^{-1}$, as extrapolated from temperature-dependent studies of immersion in PBS solution⁷⁹, compared with a dissolution rate of $\sim 90 \text{ nm d}^{-1}$ in t -SiO₂ at 96 °C (ref. 74), with a projected lifetime at 37 °C that is three orders of magnitude higher than that of a t -SiO₂ layer of encapsulation with the same thickness.

As perhaps the ultimate solution, recent work shows that monocrySTALLINE silicon carbide (SiC formed by CVD, 1,250 °C) can serve as an electrically conductive and chemically inert interface^{80–82} by physical transfer processes conceptually similar to those demonstrated for t -SiO₂. Figure 3h illustrates this concept with an NM of SiC (230 nm thick, 10^{20} cm^{-3} dopants of N, $\sim 10 \text{ k}\Omega$ impedance at 1 kHz) as a large-area biofluid barrier (area of $\sim 1 \text{ mm}^2$), with simple initial demonstrations in bioelectronics (a four-terminal resistor) interconnected by traces of gold (300 nm thick)⁸³. Helium leak tests on this SiC NM material confirm its defect-free barrier properties.

Corresponding soak tests indicate excellent water and ion barrier properties with nearly zero rates of hydrolysis (in 96 °C PBS) and ion diffusion (Na^+), thereby providing the longest operational timescale (>60 days at 96 °C) for Si-based barriers reported thus far. These materials and systems provide excellent opportunities for long-lived, flexible, high-performance bioelectronics.

Long-term implants with high resolution and scalability

The utility of these materials and integration concepts are in high-density/channel-count neural interfaces, with potential in diagnostic and neuromodulation applications capable of supporting many thousands of channels for chronic recording and stimulation. Specifically, improved resolution in recording of neural activity via μ -ECoG systems with active electronic operation can reveal high-frequency spiking activities, oscillations, microseizures and spatiotemporal patterns of behaviour, beyond the possibilities afforded by passive electrode technologies. Table 2 summarizes results for both active and passive μ -ECoG systems achieved over the past decade^{22,25,34,53,84–95}. Of note are platforms based on Si-NM transistors that offer amplification and multiplexed addressing with resolution ranging from 250 μm and 500 μm through demonstrations in rat and feline models, respectively^{22,53}, and passive electrode arrays (refer to ‘NeuroGrid’) that allow measurement of extracellular action potentials with 60 μm resolution from both rat and human cortical surfaces³⁴. A goal for future μ -ECoG systems is to achieve spatial resolution of $\sim 10 \mu\text{m}$ and temporal resolution in the submillisecond range, over large areas, all with the ability to survive without degraded performance in vivo for weeks, in the context of biomedical research and surgical diagnostics, or for many decades, in permanent implants. Such technologies demand distributed active electronic functionality, mechanical compliance, geometrical conformality and ‘perfect’ biofluid barriers.

Figure 4a,b represents a recent progress in this direction in the form of a high channel-count, flexible μ -ECoG device⁹⁵, where Si-NM arrays support active functionality for readout across more than 10^3 electrodes (28 columns, 36 rows with $330 \times 250 \mu\text{m}^2$ resolution) covering an area of $9.00 \times 9.24 \text{ mm}^2$ and encapsulated with a uniform layer of t -SiO₂. Each unit cell includes buffer and multiplexing transistors for data acquisition with only 92 wires for addressing, and sampling rates of 434 Hz per electrode channel. The resulting interconnection scheme, enabled by the electronics, offers a factor of ~ 11 times fewer wires (92) compared with passive electronic designs with the same numbers of channels (Table 2). The ultrathin format for the functional materials (200-nm-thick Si-NMs) leads to system-level thicknesses ($\sim 29 \mu\text{m}$ thick) that enable high degrees of mechanical flexibility (Fig. 4b, right) and minimal bending-induced strain associated with mounting in artificial dura (radii of curvature of $\sim 1.5 \text{ mm}$). The result allows for robust operation on the sensorimotor cortices of animal models across a range of species, including non-human primates (NHP) (Fig. 4c). The spatiotemporal dynamics results shown in Fig. 4d represent the use of such a high-resolution μ -ECoG platform to capture visual evoked biopotentials that propagate from sensory to motor cortices of an NHP. The data correspond to full electrophysiological maps with $>10^3$ sensing sites, shown here at 6 sequential time points over a period of 125 ms. Such large-scale and continuous monitoring and mapping of responses on multiple cortical surfaces have potential uses in neuroscience research and, ultimately, human health and brain interfaces.

Chronic stability is enabled by layers of t -SiO₂ (Fig. 4a) on the front and back sides, and along the lengths of the interconnecting wires for readout (Fig. 4e). Figure 4f shows the leakage currents measured from systems with these designs, but reduced in overall dimensions to allow chronic implantation on the auditory cortex of adult rats (five animals). The results indicate that the currents remain below the safety thresholds for more than a year (maximum of 435 days). In this particular case, external failure results from a

Table 2 | Performance of recent flexible μ -ECoG systems

Studies	Year	Subject	Active or passive	Number of electrodes	Number of wires	Spacing (mm)	Coverage (mm ²)	Implant duration for study
Ref. ⁸⁴	2006	Rat	Passive	64	64	0.75	36	-
Ref. ⁸⁵	2007	Rat	Passive	256	256	0.5	64	-
Ref. ⁸⁶	2007	Rat	Passive	72	72	0.64	27	42 days
Ref. ⁸⁷	2007	NHP	Passive	56	56	1	36	-
Ref. ⁸⁸	2009	NHP	Passive	252	252	2	2,100	137 days
Ref. ⁸⁹	2011	Rat	Passive	256	256	0.5	64	-
Ref. ⁹⁰	2011	Human	Passive	127	127	10	12,700	-
Ref. ²²	2011	Cat	Active	360	58	0.5	90	-
Ref. ⁹¹	2012	Human	Passive	64	64	4	1,000	-
Ref. ³⁴	2015	Rat	Passive	64	64	0.1	1	10 days
Ref. ⁵²	2014	Rat	Active	196	29	0.25	12.25	-
Ref. ⁹²	2016	Human	Passive	128	128	3	1,152	-
Ref. ⁹³	2016	Human	Passive	16	16	1	16	-
Ref. ²⁵	2016	Human	Passive	240	240	0.23	840	-
Ref. ⁹⁴	2017	NHP	Passive	96	96	0.7	4,704	-
Ref. ⁹⁵	2020	NHP	Active	1,008	92	0.33/0.25 (average 0.29)	83.16	-
		Rat	Active	64	24	0.4	10.24	435 days (in rat)

Table reproduced with permission from ref. ⁹⁵, AAAS.

sudden and irreparable detachment of the head stage and electrode from the cortical surface, suggesting the possibility that the neural interface part of the device could survive beyond this timescale. As shown in Fig. 4g, the recording of click-evoked signals (blue line) indicate SNR levels that remain above parity of 0 dB, clearly distinct from the average baseline (black line) over the course of one year (>368 days), consistent with the lifetime associated with the leakage current test (Fig. 4f). Compared with other systems (Table 2) whose lifetimes are limited by extrinsic and intrinsic properties of conventional biofluid barriers, these flexible, active electronic platforms for μ -ECoG can record stable, high-fidelity neural signals in vivo across timescales of years, due to use of defect-free t-SiO₂ encapsulation. The chronic scalability and robust, highly functional operation of this form of bioelectronic implant represent important steps toward high-performance neural interfaces that support active electronics, with capabilities for data analytics, wireless data communication and power transfer.

For use in large animal models, and ultimately, humans, scalability to areas of many square centimetres and alignment with manufacturing techniques in the integrated circuit industry will be critically important. Techniques in microscale transfer printing⁹⁶, in which soft stamps allow retrieval and delivery of large, organized collections of microscale electronic components from a source wafer to a target substrate, offer powerful capabilities in this context. Recent reports establish the basic feasibility of this type of approach, in the form of demonstrators that include heterogeneously integrated electronic/optoelectronic components, with potential to serve as large-scale, multifunctional networks for intimate interfaces to soft biotissues. An example appears in Fig. 4h,i, where assemblies of tens of thousands (>32,000) of active components (Si-NM transistors and inorganic microscale light-emitting diodes) derived from processed wafers from foundry sources are distributed at high yields (~97%; inset of Fig. 4i) and with variable pitch spacing (dense or sparse arrays, as insets in Fig. 4h) across polymer films with areas that are comparable to the full-scale dimensions of the human brain. Compared with previous reports, this example expands key metrics,

including the number of functional components (from ~2,000 to ~64,000)²¹, the number of measurement channels (from ~200 to ~32,000)⁵² and the area coverage (from ~1 cm² to 150 cm²)²². The mechanical flexibility supports bending to radii of curvature of 3 cm (Fig. 4i) after encapsulation with physically transferred barriers. The results foreshadow future 'organ scale', multifunctional bio(opto)electronic technologies with broad-ranging significance.

Challenges and future directions

As highlighted in this Review, progress in engineered materials, design constructs and integration schemes is essential to the development of flexible, long-lived bioelectronics systems with chronically stable, high-performance operation. From the standpoint of form factors, diverse options now exist, from filamentary probes to flexible sheets and open-network-mesh architectures. Various materials can be considered, although relatively few offer combined capabilities in active electronic functionality and long-term stability in operation. Recent work suggests promise in the development and use of silicon-based materials (such as Si, SiO₂, SiC, silicides) with submicrometre thicknesses derived from source wafers, as stable electrical/optical biotissue interfaces and biofluid barriers for sensing/stimulation in live animal models⁹⁷, with levels of performance and operational lifetimes that qualitatively exceed those of existing alternatives. A topic of critical importance in all cases is material biocompatibility, as immunological reactions at the material interfaces with biotissues and cells can compromise the quality of biosignals and thereby reduce the effective lifetimes of systems. In some cases, functionalized polymers and/or drug-eluting materials can suppress immunogenetic scar formation and mitigate the risks of infection. Here, and in other contexts, the notion of hybrid materials approaches that combine the best attributes of organic and inorganic materials together into integrated systems appears to represent the best approach.

Additional opportunities for research are in electronic/optoelectronic/microfluidic systems that support multifunctional operation, with options in programmed pharmacological delivery and mul-

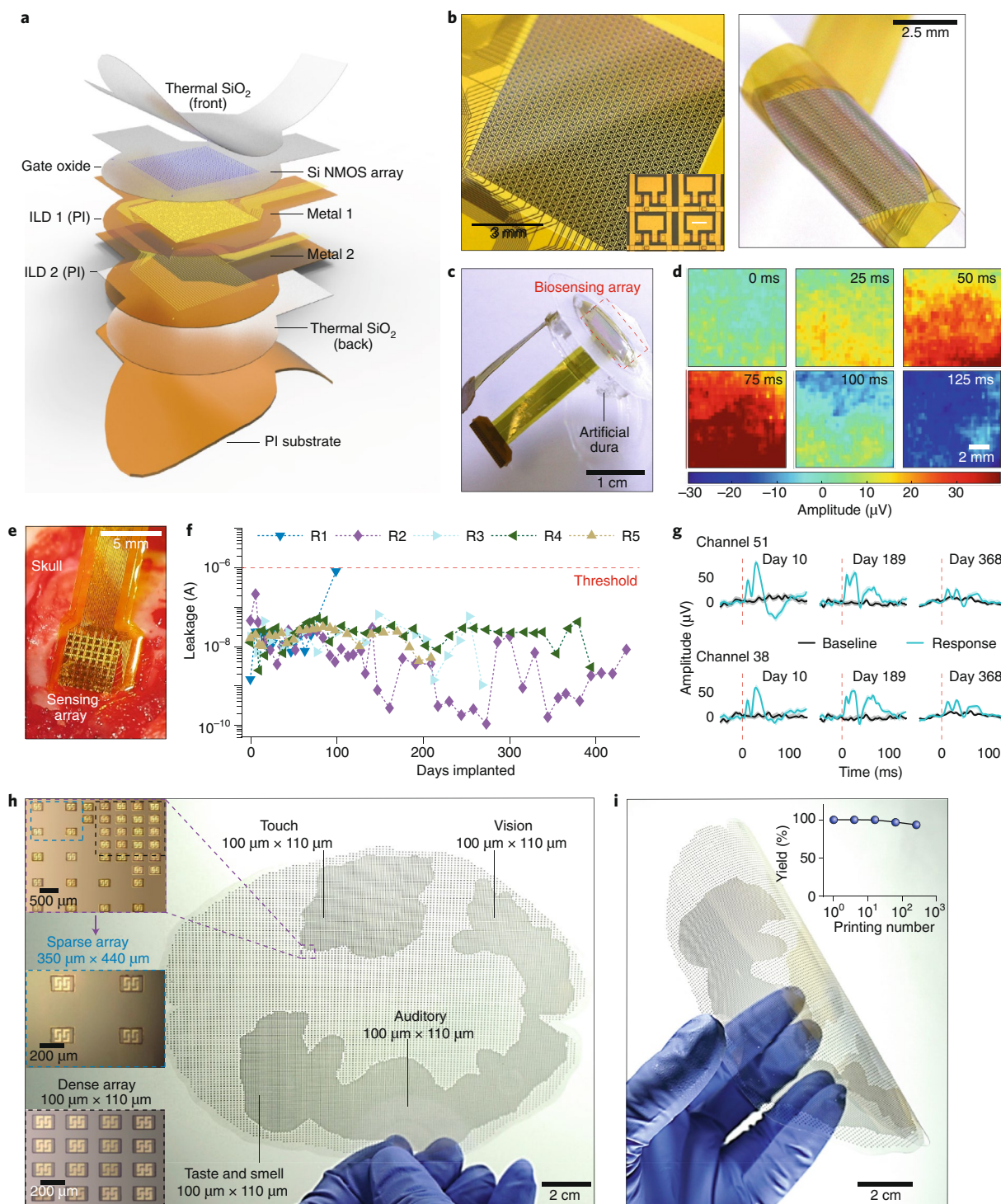


Fig. 4 | High-resolution/scalable neural electronic systems for long-term bio-integration. **a**, Schematic of a flexible bioelectronic system (n-channel metal-oxide semiconductor (NMOS) transistor array, with t-SiO₂ (900 nm thick) as encapsulation. ILD, interlayer dielectric. **b**, Image of the active region of system (>1,000 channels), in flat (left) and bent (right) states. Inset is an image of four representative unit cells in the backplane electronics. Scale bar, 100 μm. **c**, Measurement system and interconnects integrated with a soft artificial dura as a subdural interface on the sensorimotor cortices of NHP. **d**, Dynamics of visual evoked biopotential with -10³ sites on a cortical surface of a monkey. **e**, Scalable system implanted onto the auditory cortex of a rat, with t-SiO₂ encapsulation. **f**, Leakage current at various intervals during chronic operation in rat models (R1–R5). The safety threshold is 1 μA. **g**, Click-evoked response at two nodes on different days, within 368 days after implantation. Black line, average baseline; blue line, evoked potential. **h,i**, Microscale electronic components as sensing nodes on a polymer substrate in the approximate shape of a human brain, in flat (**h**) and bent (**i**) states. **h**, Insets show images (top) at regions with different densities, with magnified images (middle and bottom insets) of sparse and dense areas, respectively. **i**, The inset shows the yield (percentage of functional devices) as a function of total printing cycles. Panels reproduced with permission from: **a–g**, ref. ⁹⁵, AAAS; **h,i**, ref. ⁹⁶, PNAS.

timodal sensing, to combine measurement and diagnostics with stimulation and therapy, as the basis for closed-loop operation at different interface points (spinal cord, peripheral nerves, cardiac surfaces and other organs)^{23,38}. In all cases, biocompatible mechanics is essential, where flexibility (such as capacity to bend to small radii of curvature without damage) can be valuable but stretchability (such as capacity to stretch to large levels of strain without damage) is preferred to allow systems to adapt to natural curved textures and time dynamic motions of living systems. Considerable challenges remain in the development of collections of active and passive materials that meet all of the demanding criteria discussed in this Review, even during bending, stretching and twisting. As an additional thought, although the content presented here focuses on goals in ‘infinite’ lifetime, notable materials opportunities exist in systems that offer the opposite behaviour, as temporary implants built around concepts in ‘transient electronics’⁹⁸, where the resulting systems dissolve in biofluids to biocompatible end products with targeted lifetimes that match specific biological processes.

Many of the emerging technologies and materials for chronic neural interfaces highlighted in this Review have immediate utility in fundamental research on cell cultures, organoids and animal models, where the goal is not necessarily for use in humans. Critical challenges remain in connecting these advances to real-world applications in clinical practice, where requirements are in recording/stimulation for monitoring/treatments for neurological disorders, high spatiotemporal resolution and scalability (thousands of recording channels) for high-fidelity operation, and stable biocompatibility in terms of chemistry and mechanics for specific application cases. Efforts to address these issues focus on the constituent materials, as the basis for the next-generation of bioelectronic systems. These and other ongoing interdisciplinary efforts in neurotechnologies involve, in most cases, materials science and materials engineering at their core. The diverse topics in basic science and the potential for broad-ranging impact in biomedical research and human healthcare create fertile ground for new approaches and new concepts in fundamental and applied research.

Received: 14 November 2019; Accepted: 9 April 2020;

Published online: 27 May 2020

References

- Fang, J. Y. & Tolleason, C. The role of deep brain stimulation in Parkinson's disease: an overview and update on new developments. *Neuropsychiatr. Dis. Treat* **13**, 723–732 (2017).
- Wellman, S. M. et al. A materials roadmap to functional neural interface design. *Adv. Funct. Mater.* **28**, 1701269 (2018).
- Fu, T. M., Hong, G., Viveros, R. D., Zhou, T. & Lieber, C. M. Highly scalable multichannel mesh electronics for stable chronic brain electrophysiology. *Proc. Natl Acad. Sci. USA* **114**, E10046–E10055 (2017).
- Rivnay, J., Wang, H., Fenno, L., Delisseroth, K. & Mallaras, G. G. Next-generation probes, particles, and proteins for neural interfacing. *Sci. Adv.* **3**, e1601649 (2017).
- Berényi, A. et al. Large-scale, high-density (up to 512 channels. recording of local circuits in behaving animals). *J. Neurophysiol.* **111**, 1132–1149 (2014).
- Robinson, J. T. et al. Vertical nanowire electrode arrays as a scalable platform for intracellular interfacing to neuronal circuits. *Nat. Nanotechnol.* **7**, 180–184 (2012).
- Ershad, F., Sim, K., Thukral, A., Zhang, Y. S. & Yu, C. Invited article: emerging soft bioelectronics for cardiac health diagnosis and treatment. *APL Mater.* **7**, 031301 (2019).
- Gassert, R. & Dietz, V. Rehabilitation robots for the treatment of sensorimotor deficits: a neurophysiological perspective. *J. Neuroeng. Rehabil.* **15**, 46 (2018).
- Sanders, R. S. & Lee, M. T. Implantable pacemakers. *Proc. IEEE* **84**, 480–486 (1996).
- Mayberg, H. S. et al. Deep brain stimulation for treatment-resistant depression. *Neuron* **45**, 651–660 (2005).
- Rousche, P. J. & Normann, R. A. Chronic recording capability of the Utah intracortical electrode array in cat sensory cortex. *J. Neurosci. Methods* **82**, 1–15 (1998).
- Hiremath, S. V. et al. Human perception of electrical stimulation on the surface of somatosensory cortex. *PLoS ONE* **12**, e0176020 (2017).
- Vetter, R. J., Williams, J. C., Hetke, J. F., Nunamaker, E. A. & Kipke, D. R. Chronic neural recording using silicon-substrate microelectrode arrays implanted in cerebral cortex. *IEEE Trans. Biomed. Eng.* **51**, 896–904 (2004).
- Wark, H. A. C. et al. A new high-density (25 electrodes/mm²) penetrating microelectrode array for recording and stimulating sub-millimeter neuroanatomical structures. *J. Neural Eng.* **10**, 045003 (2013).
- Bouton, C. E. et al. Restoring cortical control of functional movement in a human with quadriplegia. *Nature* **533**, 247–250 (2016).
- Pandarinath, C. et al. High performance communication by people with paralysis using an intracortical brain–computer interface. *eLife* **6**, e18554 (2017).
- Bai, Q., Wise, K. D. & Anderson, D. J. A high-yield microassembly structure for three-dimensional microelectrode arrays. *IEEE Trans. Biomed. Eng.* **47**, 281–289 (2000).
- Dai, X., Zhou, W., Gao, T., Liu, J. & Lieber, C. M. Three-dimensional mapping and regulation of action potential propagation in nanoelectronics innervated tissues. *Nat. Nanotechnol.* **11**, 776–782 (2016).
- Montgomery, K. L. et al. Wirelessly powered, fully internal optogenetics for brain, spinal and peripheral circuits in mice. *Nat. Methods* **12**, 969–974 (2015).
- Canales, A. et al. Multifunctional fibers for simultaneous optical, electrical and chemical interrogation of neural circuits in vivo. *Nat. Biotechnol.* **33**, 277–284 (2015).
- Viventi, J. et al. A conformal, bio-interfaced class of silicon electronics for mapping cardiac electrophysiology. *Sci. Transl. Med.* **2**, 24ra22 (2010).
- Viventi, J. et al. Flexible, foldable, actively multiplexed, high-density electrode array for mapping brain activity in vivo. *Nat. Neurosci.* **14**, 1599–1605 (2011).
- Minev, I. R. et al. Electronic dura mater for long-term multimodal neural interfaces. *Science* **347**, 159–163 (2015).
- Tian, B. et al. Three-dimensional, flexible nanoscale field-effect transistors as localized bioprobes. *Science* **329**, 830–834 (2010).
- Khodagholy, D. et al. Organic electronics for high-resolution electrocorticography of the human brain. *Sci. Adv.* **2**, e1601027 (2016).
- Park, J.-S., Chae, H., Chung, H. K. & Lee, S. I. Thin film encapsulation for flexible AM-OLED: a review. *Semicond. Sci. Technol.* **26**, 034001 (2011).
- Xie, X., Ritch, L., Mccrugu, S., Tathircddy, P. & Solzbacher, F. Plasma-assisted atomic layer deposition of Al₂O₃ and parylene C bi-layer encapsulation for chronic implantable electronics. *Appl. Phys. Lett.* **101**, 093702 (2012).
- Luan, L. et al. Ultraflexible nanoelectronic probes form reliable, glial scar-free neural integration. *Sci. Adv.* **3**, e1601966 (2017).
- Musk, E. An integrated brain–machine interface platform with thousands of channels. *J. Med. Internet. Res.* **21**, e16194 (2019).
- McCallum, G. A. et al. Chronic interfacing with the autonomic nervous system using carbon nanotube (CNT) yarn electrodes. *Sci. Rep.* **7**, 11723 (2017).
- Yang, X. et al. Bioinspired neuron-like electronics. *Nat. Mater.* **18**, 510–517 (2019).
- Kozai, T. D. Y. et al. Ultrasmall implantable composite microelectrodes with bioactive surfaces for chronic neural interfaces. *Nat. Mater.* **11**, 1065–1073 (2012).
- Wang, L. et al. Ultrasoft and highly stretchable hydrogel optical fibers for in vivo optogenetic modulations. *Adv. Opt. Mater.* **6**, 1800427 (2018).
- Khodagholy, D. et al. NeuroGrid: recording action potentials from the surface of the brain. *Nat. Neurosci.* **18**, 310–315 (2015).
- Lee, W. et al. Nonthrombogenic, stretchable, active multielectrode array for electroanatomical mapping. *Sci. Adv.* **4**, eaau2426 (2018).
- Campana, A. et al. Electrocardiographic recording with conformable organic electrochemical transistor fabricated on resorbable bioscaffold. *Adv. Mater.* **26**, 3874–3878 (2014).
- Zhang, Y. C. et al. Climbing-inspired twining electrodes using shape memory for peripheral nerve stimulation and recording. *Sci. Adv.* **5**, eaaw1066 (2019).
- Borschel, G. H., Kia, K. F., Kuzon, W. M. Jr & Dennis, R. G. Mechanical properties of acellular peripheral nerve. *J. Surg. Res.* **114**, 133–139 (2003).
- Kim, D.-H. et al. Dissolvable films of silk fibroin for ultrathin conformal bio-integrated electronics. *Nat. Mater.* **9**, 511–517 (2012).
- Liu, J. et al. Syringe-injectable electronics. *Nat. Nanotechnol.* **10**, 629–636 (2015).
- Yan, Z. et al. Three-dimensional mesostructures as high-temperature growth templates, electronic cellular scaffolds, and self-propelled microrobots. *Proc. Natl Acad. Sci. USA* **114**, E9455–E9464 (2017).
- Bhunias, S., Majerus, S. & Sawan, M. *Implantable Biomedical Microsystems: Design Principles and Applications* (Elsevier, 2015).
- Johnson, L. A. et al. Direct electrical stimulation of the somatosensory cortex in humans using electrocorticography electrodes: a qualitative and quantitative report. *J. Neural Eng.* **10**, 036021 (2013).
- Waziri, A. et al. Initial surgical experience with a dense cortical microarray in epileptic patients undergoing craniotomy for subdural electrode implantation. *Neurosurgery* **64**, 540–545 (2009).

45. Khodagholy, D. et al. In vivo recordings of brain activity using organic transistors. *Nat. Commun.* **4**, 1575 (2013).
46. Kaltenbrunner, M. et al. An ultra-lightweight design for imperceptible plastic electronics. *Nature* **499**, 458–463 (2013).
47. Jun, J. J. et al. Fully integrated silicon probes for high-density recording of neural activity. *Nature* **551**, 232–236 (2017).
48. Lopez, C. M. et al. An implantable 455-active-electrode 52-channel CMOS neural probe. *IEEE J. Solid-State Circuits* **49**, 248–261 (2014).
49. Tian, B. et al. Macroporous nanowire nanoelectronic scaffolds for synthetic tissues. *Nat. Mater.* **11**, 986–994 (2012).
50. Xie, C. et al. Three-dimensional macroporous nanoelectronic networks as minimally invasive brain probes. *Nat. Mater.* **14**, 1286–1293 (2015).
51. Patel, S. R. & Lieber, C. M. Precision electronic medicine in the brain. *Nat. Biotechnol.* **37**, 1007–1012 (2019).
52. Escabi, M. A. et al. A high-density, high-channel count, multiplexed mu ECoG array for auditory-cortex recordings. *J. Neurophysiol.* **112**, 1566–1583 (2014).
53. Hwang, G.-T. et al. In vivo silicon-based flexible radio frequency integrated circuits monolithically encapsulated with biocompatible liquid crystal polymers. *ACS Nano* **7**, 4545–4553 (2013).
54. Sim, K., Rao, Z., Li, Y., Yang, D. & Yu, C. Curvy surface conformal ultra-thin transfer printed Si optoelectronic penetrating microprobe arrays. *npi Flex. Electron* **2**, 2 (2018).
55. Patzold, R., Winnacker, A., Henseler, D., Cesari, V. & Heuser, K. Permeation rate measurements by electrical analysis of calcium corrosion. *Rev. Sci. Instrum.* **74**, 5147–5150 (2003).
56. Choi, M.-C., Kim, Y. & Ha, C.-S. Polymers for flexible displays: from material selection to device applications. *Prog. Polym. Sci.* **33**, 581–630 (2008).
57. Debeaufort, F., Voilley, A. & Meares, P. Water vapor permeability and diffusivity through methylcelluloseseeded films. *J. Membrane. Sci.* **91**, 125–133 (1994).
58. Ahmad, J., Bazaka, K., Anderson, L. J., White, R. D. & Jacob, M. V. Materials and methods for encapsulation of OPV: a review. *Renew. Sustain. Energy Rev* **27**, 104–117 (2013).
59. McKeen, L. W. Permeability Properties of Plastics and Elastomers (Elsevier, 2016).
60. Groner, M. D., George, S. M., McLean, R. S. & Garcia, P. F. Gas diffusion barriers on polymers using Al₂O₃ atomic layer deposition. *Appl. Phys. Lett.* **88**, 051907 (2006).
61. Yasuda, H. & Stannett, V. Permeation, solution, and diffusion of water in some high polymers. *J. Polym. Sci.* **57**, 907–923 (1962).
62. Feng, J., Berger, K. R. & Douglas, E. P. Water vapor transport in liquid crystalline and non-liquid crystalline epoxies. *J. Mater. Sci.* **39**, 3413–3423 (2004).
63. Barrie, J. A. & Machin, D. The sorption and diffusion of water in silicone rubbers. Part II. *Filled rubbers. J. Macromol. Sci. B* **3**, 673–692 (1969).
64. Davis, E. M., Benetators, N. M., Regnault, W. F., Winey, K. I. & Elabd, Y. A. The influence of thermal history on structure and water transport in parylene C coatings. *Polymer* **52**, 5378–5386 (2011).
65. Seo, S.-W. et al. Moisture permeation through ultrathin TiO₂ films grown by atomic layer deposition. *Appl. Phys. Express* **5**, 035701 (2012).
66. Nagai, S. Approximation of effective moisture-diffusion coefficient to characterize performance of a barrier coating. *J. Appl. Phys.* **114**, 174302 (2013).
67. Yu, D., Yang, Y.-Q., Chen, Z., Tao, Y. & Liu, Y.-F. Recent progress on thin-film encapsulation technologies for organic electronic devices. *Opt. Commun.* **362**, 43–49 (2016).
68. Meyer, J. et al. Al₂O₃/ZrO₂ nanolaminates as ultrahigh gas-diffusion barriers — a strategy for reliable encapsulation of organic electronics. *Adv. Mater.* **21**, 1845–1849 (2009).
69. Fang, H. et al. Capacitively coupled arrays of multiplexed flexible silicon transistors for long-term cardiac electrophysiology. *Nat. Biomed. Eng.* **1**, 0038 (2017).
70. Lopez, C. M. et al. A neural probe with up to 966 electrodes and up to 384 configurable channels in 0.13 μm SOI CMOS. *IEEE Trans. Biomed. Circuits Syst.* **11**, 510–522 (2017).
71. Song, E., Li, J. & Rogers, J. A. Barrier materials for flexible bioelectronic implants with chronic stability-current approaches and future directions. *APL Mater.* **7**, 050902 (2019).
72. Oehler, A. & Tomozawa, M. Water diffusion into silica glass at a low temperature under high water vapor pressure. *J. Non. Cryst. Solids* **347**, 211–219 (2004).
73. Lin, Y., Tsui, T. Y. & Vlassak, J. J. Water diffusion and fracture in organosilicate glass film stacks. *Acta Mater.* **55**, 2455–2464 (2007).
74. Fang, H. et al. Ultrathin, transferred layers of thermally grown silicon dioxide as biofluid barriers for biointegrated flexible electronic systems. *Proc. Natl Acad. Sci. USA* **113**, 11682–11687 (2016).
75. Song, E. et al. Thin, transferred layers of silicon dioxide and silicon nitride as water and ion barriers for implantable flexible electronic systems. *Adv. Electron. Mater.* **3**, 1700077 (2017).
76. Song, E. et al. Ultrathin trilayer assemblies as long-lived barriers against water and ion penetration in flexible bioelectronic systems. *ACS Nano* **12**, 10317–10326 (2018).
77. Li, J. et al. Conductively coupled flexible silicon electronic systems for chronic neural electrophysiology. *Proc. Natl Acad. Sci. USA* **115**, E9542–E9549 (2018).
78. Lee, Y. K. et al. Dissolution of monocrystalline silicon nanomembranes and their use as encapsulation layers and electrical interfaces in water-soluble electronics. *ACS Nano* **11**, 12562–12572 (2017).
79. Li, J. et al. Ultrathin, transferred layers of metal silicide as faradaic electrical interfaces and biofluid barriers for flexible bioelectronic implants. *ACS Nano* **13**, 660–670 (2019).
80. Cogan, S. F., Edell, D. J., Guzelian, A. A., Liu, Y. P. & Edell, R. Plasma-enhanced chemical vapor deposited silicon carbide as an implantable dielectric coating. *J. Biomed. Mater. Res. A* **67a**, 856–867 (2003).
81. Knaack, G. L. et al. In vivo characterization of amorphous silicon carbide as a biomaterial for chronic neural interfaces. *Front. Neurosci.* **10**, 301 (2016).
82. Lei, X. et al. SiC protective coating for photovoltaic retinal prosthesis. *J. Neural. Eng.* **13**, 046016 (2016).
83. Phan, H.-P. et al. Long-lived, transferred crystalline silicon carbide nanomembranes for implantable flexible electronics. *ACS Nano* **13**, 11572–11581 (2019).
84. Hollenberg, B. A., Richards, C. D., Richards, R., Bahr, D. F. & Rector, D. M. A MEMS fabricated flexible electrode array for recording surface field potentials. *J. Neurosci. Methods* **153**, 147–153 (2006).
85. Benison, A. M., Rector, D. M. & Barth, D. S. Hemispheric mapping of secondary somatosensory cortex in the rat. *J. Neurophysiol.* **97**, 200–207 (2007).
86. Molina-Luna, K. et al. Cortical stimulation mapping using epidurally implanted thin-film microelectrode arrays. *J. Neurosci. Methods* **161**, 118–125 (2007).
87. Kim, J., Wilson, J. A. & Williams, J. C. A cortical recording platform utilizing μECoG electrode arrays. In *2007 29th Annual International Conference of the IEEE Engineering in Medicine and Biology Society* 5353–5357 (IEEE, 2007).
88. Rubehn, B., Bosman, C., Oostenveld, R., Fries, P. & Stieglitz, T. A MEMS-based flexible multichannel ECoG-electrode array. *J. Neural Eng.* **6**, 036003 (2009).
89. Ledochowitsch, P. et al. Fabrication and testing of a large area, high density, parylene MEMS μECoG array. In *2011 IEEE 24th International Conference on Micro Electro Mechanical Systems* 1031–1034 (IEEE, 2011).
90. Besle, J. et al. Tuning of the human neocortex to the temporal dynamics of attended events. *J. Neurosci.* **31**, 3176–3185 (2011).
91. Pasley, B. N. et al. Reconstructing speech from human auditory cortex. *PLoS Biol.* **10**, e1001251 (2012).
92. Hotson, G. et al. Individual finger control of a modular prosthetic limb using high-density electrocorticography in a human subject. *J. Neural Eng.* **13**, 026017 (2016).
93. Kellis, S. et al. Multi-scale analysis of neural activity in humans: implications for micro-scale electrocorticography. *Clin. Neurophysiol.* **127**, 591–601 (2016).
94. Kaiju, T. et al. High spatiotemporal resolution ECoG recording of somatosensory evoked potentials with flexible micro-electrode arrays. *Front. Neural Circuits* **11**, 20 (2017).
95. Chiang, C.-H. et al. The neural matrix: kiloscale neural interfaces for long-term recording. *Sci. Transl. Med.* **12**, eaay4682 (2020).
96. Song, E. et al. Flexible electronic/optoelectronic microsystems with scalable designs for chronic biointegration. *Proc. Natl Acad. Sci. USA* **116**, 15398–15406 (2019).
97. Lee, W. et al. Transparent, conformable, active multielectrode array using organic electrochemical transistors. *Proc. Natl Acad. Sci. USA* **114**, 10554–10559 (2017).
98. Yu, K. J. et al. Bioresorbable silicon electronics for transient spatiotemporal mapping of electrical activity from the cerebral cortex. *Nat. Mater.* **15**, 782–791 (2016).

Acknowledgements

We acknowledge support from the Querrey Simpson Institute for Bioelectronics at Northwestern University.

Competing interests

The authors declare no competing interests.

Additional information

Correspondence should be addressed to J.A.R.

Reprints and permissions information is available at www.nature.com/reprints.

Publisher's note Springer Nature remains neutral with regard to jurisdictional claims in published maps and institutional affiliations.

© Springer Nature Limited 2020